Current Molecular Pharmacology, 2017, *10*, 334-344

RESEARCH ARTICLE

Decoding Corticotropin-Releasing Factor Receptor Type 1 Crystal Structures

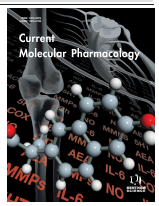

Andrew S. Doré[1], Andrea Bortolato[1], Kaspar Hollenstein[2], Robert K.Y. Cheng[1], Randy J. Read[3] and Fiona H. Marshall[1,*]

[1]*Heptares Therapeutics Ltd, BioPark, Broadwater Road, Welwyn Garden City, Herts, AL7 3AX, UK;* [2]*Merck Research Laboratories, West Point, PA 19486, USA;* [3]*Dept. of Haematology, University of Cambridge, Cambridge Institute for Medical Research, Wellcome Trust/MRC Building, Hills Road, Cambridge, CB2 0XY, UK*

ARTICLE HISTORY

Received: June 16, 2016
Revised: August 03, 2016
Accepted: August 03, 2016

DOI:
10.2174/1874467210666170110114727

Abstract: The structural analysis of class B G protein-coupled receptors (GPCR), cell surface proteins responding to peptide hormones, has until recently been restricted to the extracellular domain (ECD). Corticotropin-releasing factor receptor type 1 (CRF_1R) is a class B receptor mediating stress response and also considered a drug target for depression and anxiety. Here we report the crystal structure of the transmembrane domain of human CRF_1R in complex with the small-molecule antagonist CP-376395 in a hexagonal setting with translational non-crystallographic symmetry. Molecular dynamics and metadynamics simulations on this novel structure and the existing TMD structure for CRF_1R provides insight as to how the small molecule ligand gains access to the induced-fit allosteric binding site with implications for the observed selectivity against CRF_2R. Furthermore, molecular dynamics simulations performed using a full-length receptor model point to key interactions between the ECD and extracellular loop 3 of the TMD providing insight into the full inactive state of multidomain class B GPCRs.

Keywords: CRF1R, translational non-crystallographic symmetry, molecular dynamics, GPCR, metadynamics, CP-376395.

1. INTRODUCTION

The secretin subfamily of Class B G protein-coupled receptors (GPCRs) includes many important and clinically validated drug targets. These include the glucagon like peptide receptor GLP1 for diabetes, calcitonin gene related peptide receptor for migraine and the parathyroid hormone receptor PTH1 for osteoporosis [1]. Corticotropin releasing factor receptor (CRF_1R) itself is an important drug target across a range of different disease areas outlined elsewhere in accompanying chapters. In particular a focus of interest for many years by pharmaceutical companies is its role in stress related disorders such as depression [2]. Despite extensive efforts, Class B GPCRs have proved very intractable as drug targets and to date no small molecule modulators have reached the market. The CRF_1 receptor is one of the few Class B receptors where small molecule antagonists, such as CP-376395 have been identified by high throughput screening [3]. In order to fully understand the precise mechanism of action of CP-376395 we set out to solve the X-ray structure of the CRF_1R bound to CP-376395.

Major technological advances in the area of protein expression, purification and crystallization together with techniques to address the lack of stability and conformational flexibility of GPCRs have enabled the structures of over 20 Class A receptors to be solved. However, structures of Class B GPCRs have lagged behind. This is due in part to the lack of small molecule ligands for co-crystallization and the multi-domain architecture of class B GPCRs consisting of the membrane spanning 7-transmembrane domain and the extracellular peptide ligand binding domain. GPCR crystal structures are highly enabling for structure based drug design approaches [4] and also permitting homology models to be built for related receptors. However X-ray structures represent a 'snap-shot' of one particular conformation of the protein/ligand complex providing limited information on the flexibility of the protein and no information relating to the dynamics of ligand binding. Molecular dynamic (MD) simulations are increasingly being applied to study GPCRs and are being actively used in drug design to provide information on the dynamics of conformational changes by the receptor as well as the complex interplay between the protein, water networks and ligand receptor interactions [5]. Here we have also used MD and metadynamics simulations to study ligand receptor interactions in CRF_1R and the conformational changes which may occur in the full length receptor.

*Address correspondence to this author at the Heptares Therapeutics Ltd, BioPark, Broadwater Road, Welwyn Garden City, Herts, AL7 3AX, UK; Tel: +44 1707 358637; Fax: +44 1707 358640; E-mail: fiona.marshall@heptares.com

1874-4702/17 $58.00+.00

2. MATERIALS AND METHODS

2.1. Protein Expression and Purification

The full-length human CRF_1R with an intact ICL2 (no T4L insertion) was used as background for generation of the StaR using a mutagenesis approach described previously and mutants analyzed for thermostability in the presence of the selective radioligand [^{3}H]CP-376395. While wild type CRF_1R displayed an apparent thermostability (Tm) of 18.4 °C (±2.0 °C) in *n*-dodecyl-β-D-maltopyranoside (DDM), the CRF_1R StaR (full-length receptor with 12 thermostabilizing mutations) displayed a Tm of 44.7 °C (±2.2 °C) in an identical assay, dropping to a Tm of 37.5 °C (±0.7 °C) upon fusion of the T4L. The CRF_1R-TMD carrying a T4 lysozyme fusion in intracellular loop 2 and a C-terminal deca-histidine tag was expressed in *Trichoplusia ni* (High Five) cells in EX-CELL 405 medium (Sigma-Aldrich) supplemented with 10 % (v/v) fetal bovine serum (Sigma-Aldrich), 1 % (v/v) CD lipid concentrate (GIBCO) and 1 % (v/v) Penicillin/Streptomycin (PAA Laboratories). Cells were infected at a density of 2 x 10^6 cells/ml with 10 ml of baculovirus per liter of culture, corresponding to an approximate multiplicity of infection (MOI) of 1. Cultures were grown at 27 °C with constant shaking and harvested 72 hours post infection. Cells were pelleted and washed with 250 ml PBS and stored at -80 °C. All subsequent purification steps were carried out at 4 °C unless indicated differently. To prepare membranes, cells were thawed at room temperature and resuspended in 400 ml ice-cold 50 mM Tris-HCl pH 8.0, 500 mM NaCl supplemented with EDTA-free protease inhibitors (Roche). The cell suspension was incubated with 0.3 µM CP376395 (Tocris) for 1 hour to allow the ligand to bind. Cells were disrupted by ultra-sonication and cell debris was removed by centrifugation at 10.000 x *g*. Membranes were collected by ultracentrifugation at 140.000 x *g*, resuspended and stored at -80 °C until further use. Membranes were thawed at room temperature and solubilized with 2 % (w/v) DM for 1.5 hours. Insoluble material was removed by ultracentrifugation and the receptors were immobilized by batch binding to TALON metal-affinity resin (Clontech) for 2 hours. The resin was packed into a XK-16 column (GE Healthcare) and washed with steps of 8 and 30 mM imidazole in 50 mM Tris-HCl pH 8.0, 500 mM NaCl, 0.15 % (w/v) DM, and 0.3 µM CP376395 for a total of 15-20 column volumes before bound material was eluted with 200 mM imidazole. The protein was then concentrated using an Amicon Ultra-15 centrifugal filter unit (Millipore) and subjected to preparative gel filtration in 20 mM Tris-HCl pH 8.0, 150 mM NaCl, 0.15 % (w/v) DM, and 0.3 µM CP376395 on a Superdex 200 10/300 GL gel filtration column (GE Healthcare) to remove remaining contaminating proteins and aggregates. Receptor purity was analyzed using SDS-PAGE and mass spectrometry and receptor monodispersity was assayed by FSEC monitoring tryptophan fluorescence. Protein concentration was determined with a NanoDrop spectrophotometer using the receptor's calculated extinction coefficient at 280 nm ($e_{280, calc}$ = 1.6 (mg/ml x cm)$^{-1}$).

2.2. Crystallization

The CRF_1R-TMD was crystallized in lipidic cubic phase (LCP) at 22.5 °C. The protein was concentrated to 20-30 mg/ml by ultrafiltration and mixed with monoolein (Nu-Check) supplemented with 10 % (w/w) cholesterol (Sigma) and 5 µM CP376395 using the twin-syringe method [6] with a final protein:lipid ratio of 1:1.5 (w/w). A Mosquito LCP (TTP Labtech) was used to dispense 40-60 nl boli on 96-well Laminex Glass Bases (Molecular Dimensions), overlaid with 0.75 µl precipitant solution and sealed with Laminex Film Covers (Molecular Dimensions). 20-30 µm crystals of construct CRF_1R-#76 were obtained in 100 mM Na-citrate pH 5.5, 200 mM Li_2SO_4, 30 % (v/v) polyethylene glycol 400, 0.6 µM CP376395. Crystals were flash cooled in liquid nitrogen without additional cryoprotectant.

2.3. Diffraction Data Collection and Processing

X-ray diffraction data were measured on a Pilatus 6M hybrid-pixel detector at Diamond Light Source beamline I24 using a 5 µm diameter microbeam. Crystals displayed isotropic diffraction to beyond 3.0 Å following exposure to an unattenuated beam for 8 seconds per degree of oscillation. Consequently radiation damage set in quickly and less than 5 degrees of oscillation data per crystal could be used in subsequent data merging. Data from individual crystals were integrated using *XDS* [7]. The final dataset included data from 21 crystals (with reindexing as required) and was scaled to 3.18 Å using the microdiffraction assembly method as described previously [8, 9] with a final overall completeness of 93.7 %. Crystals belonged to hexagonal space group *P6* with unit cell dimension of a = b = 189.4 Å, c = 88.6 Å, α = β = 90 ° γ = 120 °. The resulting multi-record reflection file was scaled using *AIMLESS* from the CCP4 suite [10, 11]. Data collection statistics are presented in Table **1**.

2.4. Structure Solution and Refinement

The CRF_1R-#76 crystals belong to hexagonal space group *P6* exhibiting a 30 % off-origin peak in a native Patterson map, indicating translational non-crystallographic symmetry (tNCS). Previously, it was possible to modulate the construct in terms of the TMD and T4 Lysozyme (T4L) linker resulting in construct CRF_1R-#105 which crystallized in the same conditions as CRF_1R-#76 yet belonged to an orthorhombic spacegroup displaying no tNCS and which was subsequently solved and refined (PDB ID: 4K5Y) [9]. The structure of CRF_1R-#76 was solved by molecular replacement (MR) with the program *Phaser* [12] utilising corrections for the statistical effects of tNCS function [13] with two independent search models, T4L from CRF_1R and the TMD of CRF_1R (PDB ID 4K5Y). Solutions were found for all three copies of the T4L and TMD in the asymmetric unit.

The nature of the tNCS was unusual. The peak in the native Patterson map indicated a tNCS translation of approximately 1/3,2/3,0, from which one might expect three copies in the asymmetric unit to be generated by successive applications of the same translation vector, corresponding to an approximate tripling of a smaller unit cell. However, the tNCS likelihood target [13] was about 1600 units higher when assuming two tNCS-related copies instead of three. A molecular replacement search for two copies each of the TMD and T4L models gave an unambiguous solution, in which a crystallographic 3-fold axis generated hexamers from the two copies. The crystal packing left a hole around

the crystallographic 6-fold axis, sufficient to place an additional copy generating a hexamer, but surprisingly the molecular replacement search for an additional copy each of the TMD and T4L placed them in an inverted orientation, so the third copy was not in fact related by translation to the first two.

Manual model building was performed in *COOT* [14] using sigma-A weighted $2m|F_o|-|DF_c|$, $m|F_o|-D|F_c|$ maps calculated using *Phenix* [15]. Initial refinement was carried out with *REFMAC5* [11, 16] using maximum-likelihood restrained refinement in combination with the jelly-body protocol. Late stages of the refinement were performed with *Phenix.refine* [17] with positional and individual isotropic B-factor refinement and *TLS*. The structure was validated using *MolProbity* [18]. The final refinement statistics are presented in Table **1**. Figures were prepared using *PyMOL* [19].

2.5. Structural Analysis

Cα RMSD calculation between different copies of the CRF_1R-TMD structures was performed using *Superpose* [11]. The following amino-acid ranges were used 125-140(TM1), 154-164(TM2), 190-209(TM3), 241-249(TM4), 272-291(TM5), 314-322(TM6) and 350-365(TM7).

2.6. Molecular Dynamics Simulation

The three dimensional coordinates of CRF_1R (space group $P22_12_1$, CRF_1R^{P22121}) in complex with the small molecule antagonist CP-376395 [9] were downloaded from the Protein Data Bank [20]. The receptor was prepared with the Protein Preparation Wizard in Maestro [21]: only the protein and the ligand in chain C have been included, hydrogen atoms have been added and the H-bond network has been optimized through an exhaustive sampling of hydroxyl and thiol moieties, tautomeric and ionic state of His and 180° rotations of the terminal dihedral angle of amide groups of Asp and Gln. $His155^{2.50}$ has been considered to be protonated. Hydrogen atoms have been energy minimized using the OPLS2.1 force field. The same protocol has been applied to chain A of CRF_1R in the hexagonal space group P6 (CRF_1R^{P6}), while for the MD simulation of the apo state of CRF_1R^{P22121} the ligand CP-376395 has been deleted. The homology model of the receptor including the extracellular domain (ECD-CRF_1R^{P22121}) has been created using CRF_1R^{P22121} chain A for the TMD and the crystal structure of the N-terminal extracellular domain available in the Protein Data Bank (PDB ID: 3EHS) [22]. The 6 residues missing between the two crystal structures (from E109 to V114) have been assumed to be helical creating one and half helical turn connecting the top of TM1 helix to the helix at the end of the ECD. The continuous helical nature of the link between the two domains determined their final relative orientation. The T4L has been removed, the ICL2 conformation has been predicted using Prime [23] and the final system has been prepared with the same protocol described above with the Protein Preparation Wizard in Maestro.

The 4 prepared systems (CRF_1R^{P22121}, CRF_1R^{P6}, apo CRF_1R^{P22121} and ECD-CRF_1R^{P22121}) have been analysed using standard MD simulations with the following protocol. The AMBER99SB force field (ff) [24] parameters were used for the protein and the GAFF ff [25] for the ligands using AM1-BCC partial charges [26]. The system has been embedded in a triclinic box including an equilibrated membrane consisting of 256 DMPC (1,2-dimyristoyl-sn-glycero-3-phosphocholine) lipids [27] and 24513 waters using g_membed [28] in GROMACS (v4.6.5). The SPC water model was used and ions were added to neutralize the system (final concentration 0.01 M). CRF_1R^{P22121} included a total of 103,468 atoms (24,233 water molecules, 7 Na^+, 16 Cl^- and 226 lipids), while CRF_1R^{P6} was composed by 103,590 atoms (24,190 water molecules, 7 Na^+, 18 Cl^- and 226 lipids). An energy minimization protocol based on 200 steps steepest-descent algorithm followed by 500 steps conjugate gradient algorithm has been applied to the system. The membrane has been equilibrated using 2 ns MD simulation with a time step of 2.5 fs, using LINCS on all bonds and keeping the protein and ligand restrained applying a force of 100 kJ mol^{-1} nm^{-1}. Lennard-Jones and Coulomb interactions were treated with a cut-off of 1.069 nm with particle-mesh Ewald electrostatics (PME) [29]. The MD has been executed in the NPT ensemble using v-rescale [30] (tau_t = 0.5 ps) for the temperature coupling to maintain the temperature of 303 K and using Parrinello-Rahman [31] (tau_p = 10.0 ps) for the semi-isotropic pressure coupling to maintain the pressure of 1.013 bar. Finally a 50 ns MD simulation has been performed using the same settings described above, but without applying any positional restraints. The CRF_1R double mutant has been generated introducing the $His199Val^{3.40b}$ and $Met276Ile^{5.44b}$ mutations in the equilibrated system. ECD-CRF_1R^{P22121} has been generated and equilibrated with a comparable protocol and resulted in a system composed by a total of 124,752 atoms (30,717 water molecules, 8 Na^+, 17 Cl^- and 228 lipids).

2.7. Metadynamics Simulation

Well-tempered Metadynamics (WTMetaD) [32] simulations have been used to evaluate: 1) the lowest energy binding path of CP-376395 to CRF_1R^{P22121}, 2) low energy conformations of the ECD relative to the receptor TMD. All simulations have been carried out using GROMACS with the same MD protocol described above and PLUMED (v2.0.2) [33] with a time step of 2 fs.

Possible ligand binding and dissociation paths were initially generated using a steered MD [34] protocol. The method was based on 24 steps of 250 ps MD each for a total of 6 ns: 3 ns for the ligand binding and 3 ns for the dissociation event simulation, 12 steps each. Using a python script the protocol started with a target RMSD from the ligand bound conformation value of 10 Å and a force constant of 1 kJ mol^{-1} nm^{-1}. To ensure the final ligand bound state was reached, the target RMSD value was consecutively decreased and kappa increased by 10-fold in the first 12 steps. For the dissociation 12 steered MD steps with the same settings were applied using as target position the initial unbound conformation of the ligand. Two possible binding-dissociation paths for the small molecule have been considered: one accessing the ligand binding site from the extracellular side and one from the membrane. These have been achieved positioning the ligand in different starting locations at about 20 Å from the bound state, respectively in the extracellular side close to the orthosteric site and into the membrane close to TM5. The obtained binding routes have been used to define a path collective variable (CV) for the

WTMetaD with the following settings: simulated temperature 300 K, bias factor 90, initial energy bias Gaussian height of 0.3 kJ/mol with a deposition frequency of 500 MD steps. A geometric based hills width scheme [35] has been applied starting with a sigma value of 0.1. Two path collective variables have been defined [36] one defining the position on the path and the other the distance from the path. A Lambda value of 3.0 has been applied. A total of 58 ns WTMetaD starting from the ligand bound state were required to reach the lowest energy barrier allowing the ligand to dissociate from the receptor. The same procedure has been used for the study of the CRF_1R double mutant (His199Val$^{3.40b}$ and Met276Ile$^{5.44b}$).

A similar protocol has been used to identify stable "open" and "closed" conformations of the ECD relative to the receptor helical bundle. In this case the path CV has been defined using the starting and final protein conformations from the 50 ns MD of the ECD-CRF_1R^{P22121}. Two restraining potential walls have been applied to the CV describing the distance from the path at CV values of 0.3 and -0.3 (k=500 kJ mol^{-1} nm^{-1}, exp=3). Two simulations for a total of 114 ns WTMetaD starting from the "open" and "closed" ECD states have been performed. This simulation length was not sufficient to obtain a converged energy landscape of the full conformational change for the full length receptor moving from the "open" to the "closed" ECD states. The protocol described identifies representative low energy ECD conformations of the two states.

3. RESULTS

3.1. CRF_1R Crystal Structures

In 2013 the crystal structure of the TMD of CRF_1R was reported at 3.0 Å resolution [9]. CRF_1R was crystallised in Lipidic Cubic Phase (LCP) (Fig. **1**-**D**) using a conformational thermostabilisation approach to generate the stabilised receptor (StaR) and fusion of T4-Lysozyme (T4L) within intracellular loop 2 (ICL2) of the receptor to aid crystallisation (this construct is referred to as CRF_1R-#105 henceforth). The resulting structure of the human CRF_1R receptor TMD in complex with the small molecule antagonist CP-376395 (2-aryloxy-4-alkylaminopyridine) in an orthorhombic setting (referred to as CRF_1R^{P22121} henceforth) provided an exciting inaugural view of the architecture of the CRF_1R receptor and that of class B GPCRs in general.

However, these were not the first crystals of CRF_1R to be obtained. In addition to CRF_1R crystals grown using bicelles, and classical vapour diffusion (data not shown) the first generation of CRF_1R TMD crystals grown (Fig. **1**-**A**) using the *in meso* method utilised a near identical construct to CRF_1R-#105 but which incorporated two extra residues from intracellular loop 2 – one of which had been previously identified as a thermostabilising mutation (S222L) in the fusion to T4-Lysozyme (this construct is referred to as CRF_1R-#76 henceforth). The CRF_1R-#76 crystals belong to hexagonal space group *P6* exhibiting a 30 % off-origin peak in a native Patterson map, indicating translational non-crystallographic symmetry (tNCS). Although a complete dataset to 3.18 Å resolution could be generated through merging data collected from multiple crystals, extensive trials to solve the structure by molecular replacement failed, due in part to the presence of tNCS and / or the low structural similarity between search model and target. With the CRF_1R^{P22121} structure in hand it was finally possible to solve the hexagonal tNCS data (see methods) with three copies in the asymmetric unit, thereby generating a second structure of the CRF_1R receptor in complex with CP-376395 referred to as CRF_1R^{P6} henceforth (Table **1**) and which doubles the structural information available for this receptor (Fig. **1**-**B**,**C**).

Table 1. Crystallographic table of statistics.

Data Collection	
Space Group	P6
Cell Dimensions a, b, c, (Å)	189.4, 189.4, 88.6
Cell Angles α, β, γ (°)	90, 90, 120
Resolution (Å)	3.18
R_{merge}	0.158 (0.627)
I / σ I *	6.4 (1.8)
Completeness (%)	93.7 (82.0)
Redundancy	3.8 (2.5)
REFINEMENT	
Resolution (Å)	19.91 – 3.18
No. Reflections	28,393
R_{work} / R_{free}	24.4 / 28.9
No. atoms	
Protein	9,980
Ligand	264
B-factors	
Protein	90.7
Ligand	85.5
R.m.s deviations	
Bond lengths (Å)	0.006
Bond Angles (°)	0.882
Ramachandran Plot: Preferred (%)	96.4
Allowed (%)	3.4
Outlier (%)	0.2

*Statistics in parentheses refer to outer resolution shell.

Despite fundamental differences in crystal contacts / packing between the orthorhombic and hexagonal lattices, superposition of the 6 CRF_1R-TMD structures (3 copies in the asymmetric unit from both CRF_1R^{P22121} and CRF_1R^{P6}) demonstrate the structures are all in close agreement (root-mean-square deviation RMSD less than 0.4 Å across core TM residue Cα atoms – see methods) (Fig. **1**-**G**,**H**). In the hexagonal CRF_1R^{P6} crystal system interactions between receptors occur exclusively via parallel packing with TM1 and

TM7 from one receptor copy interacting with TM4 and the N-terminus of TM3 for both non-crystallographic and symmetry related copies (Fig. **1**-**C**). In the orthorhombic CRF_1R^{P22121} crystal form interactions between receptors occur in both parallel and antiparallel fashion. Parallel interactions are observed between ECL3/TM6 to ECL3/TM6, TM1 to TM1, and TM1 to TM4/N-terminus of TM3, with a single antiparallel interaction from TM4 to TM4 (Fig. **1**-**F**).

The open extracellular conformation of the peptidic agonist orthosteric pocket initially revealed in the CRF_1R^{P22121} structure is maintained across the 3 CRF_1R^{P6} copies. One side of this "chalice-like" conformation is provided by TM2-TM5, and the other by TM1, TM6, and TM7. As previously reported, in CRF_1R the slightly bent extracellular portion of TM1 packs against and stabilizes a kink in TM7 contributing to the open nature of the receptor extracellular vestibule. The highly conserved $S130^{1.50b}$ on TM1 hydrogen bonds to the backbone Nitrogen of $F357^{7.51b}$ and main-chain carbonyl of $S353^{7.47b}$, which flank $G356^{7.50b}$ on TM7. This results in the extracellular halves of TM6, TM7 and extracellular loop 3 (ECL3) tilting away from the central helical bundle [9]. Furthermore, the extracellular portions of TM6, TM7 and ECL3 (along with the N-terminus of TM1) demonstrate the highest B-factor values and structural variation across all 6 CRF_1R-TMD structures, pointing to the inherent structural flexibility of this region in CRF_1R (Fig. **1**-**I**,**J**). Indeed in only 2 of the 6 copies of the CRF_1R receptor from both the CRF_1R^{P22121} and CRF_1R^{P6} is ECL3 ordered and visible in the electron density.

Finally in all 3 copies of CRF_1R^{P6} the CP-376395 small molecule is again visible in the extraordinary position towards the intracellular side of the receptor with a single hydrogen-bond supplied by $N283^{5.50b}$, while TM3, TM5 and TM6 provide the residues that constitute the rest of the hydrophobic pocket towards the intracellular side of the receptor, as previously observed and in close agreement with the CRF_1R^{P22121} structure (Fig. **1**-**G**,**H**).

3.2. Structural Insights into CP-376395 Binding and CRF_1R Selectivity

The striking position of CP-376395 and its interactions with the receptor resulted in a very stable configuration across a 50 ns Molecular dynamics (MD) simulation within an explicit water-membrane environment. For both crystal forms (CRF_1R^{P22121} and CRF_1R^{P6}) the average ligand RMSD during simulation was ~1 Å. To evaluate whether the allosteric small-molecule binding site in CRF_1R was induced by CP-376395 we also analyzed an *apo* CRF_1R model using an identical MD simulation protocol. In this case the allosteric pocket appeared very unstable. TM6 quickly moved closer to TM3 in a position similar to that adopted in the glucagon receptor crystal structure (Fig. **2**-**A**). In particular residues $M206^{3.47b}$ and $L320^{6.46b}$ occupied and collapsed the binding site. These two residues have recently proposed to be part of the hydrophobic core of the receptor [1, 37] playing a crucial role in stabilizing the inactive receptor state by controlling the movement of the N-terminus of TM6 during activation, an essential structural prerequisite that is required for G protein docking on the intracellular surface of the receptor.

To further investigate the nature of the induced-fit CP-376395 pocket within CRF_1R, ligand binding and dissociation paths were generated using a Steered MD protocol. Two different starting positions of the small molecule were evaluated: one accessing the binding site from extracellular space; and one from within the membrane. Starting positions for CP-376395 were located ~20 Å from the crystallographic ligand bound position: in the first case this was on the extracellular side of the receptor close to the orthosteric site, while in the second it was within the membrane - in close proximity to TM5 (Fig. **2**-**B**). The Steered MD trajectories obtained were subsequently used for a well-tempered metadynamics (WTMetaD) simulation protocol starting from the bound crystallographic state. WTMetaD permitted the evaluation of the free energy surface of ligand dissociation (Fig. **2**-**C**). The most favourable and lowest energy escape route for the ligand from the induced-fit pocket was between TM5 and TM6 and towards the membrane environment. Analysis of the simulation trajectory reveals crucial movements of $F203^{3.44b}$ and $Y327^{6.53b}$ changing rotameric states during ligand dissociation (Fig. **3**-**A**,**B**). These key conformational changes permit the initial movement of the ligand from the bound crystallographic state up and towards the extracellular side of the receptor creating a high-energy transition state conformation where the H-bond between CP-376395 and $N283^{5.50}$ is broken. From this position the ligand can access the membrane between TM5 and TM6 in a location close to $G324^{6.50b}$ and $P321^{6.47b}$ (Fig. **3**-**C**). Both $G324^{6.50b}$ and $P321^{6.47b}$ contribute to a bent / flexible local conformation of TM6 to create a sterically viable exit for CP-376395 from the receptor TMD. Finally, the movement of $F203^{3.44b}$ and $Y327^{6.53b}$ during ligand dissociation (Fig. **3**-**D**) is influenced by $M276^{5.44b}$ and $H199^{3.40b}$. $M276^{5.44b}$ and $H199^{3.40b}$ have previously been demonstrated to be important for the observed selectivity of CP-376395 for CRF_1R over CRF_2R, where they are instead found to be $Ile272^{5.44b}$ and $Val195^{3.40b}$ respectively [38, 39]. To evaluate the importance of these two residues we applied the same WTMetaD protocol to the CRF_1R double mutant $His199Val^{3.40}$ $Met276Ile^{5.44}$. These mutations prevent ligand unbinding toward the membrane, creating a favourable route for unbinding in the direction of the orthosteric site (Fig. **2**-**C**). This is possibly the result of $Val199^{3.40}$ and $Ile276^{5.44}$ effecting the rotameric states of $F203^{3.44b}$ and $Y327^{6.53b}$ that are compatible (decrease the energy barrier) for ligand unbinding toward the orthosteric site. Overall the crystallographic bound state conformation is predicted 1.4 kcal/mol less stable in the double mutant compared to wild type.

3.3. Structural Insights into CRF_1R Inter-Domain Interactions

As expected, analysis of CRF_1R^{P22121} and CRF_1R^{P6} dynamic behaviour using MD simulation confirmed the conformations of both structures to be stable and in agreement. Across a 50 ns MD simulation in an explicit water-membrane environment the average RMSD for all protein Cα atoms was measured at ~2 Å. Root mean square fluctuation analysis of the trajectories highlighted a high degree of flexibility for extracellular loop 3 (ECL3) from residue N333 to E338 (Fig. **4**-**A**). This is in agreement with the high resultant B-factors and structural variation for residues in this region across both crystal forms and six receptor copies obtained for the CRF_1R-TMD (Fig. **1**-**I**,**J**). To investigate the

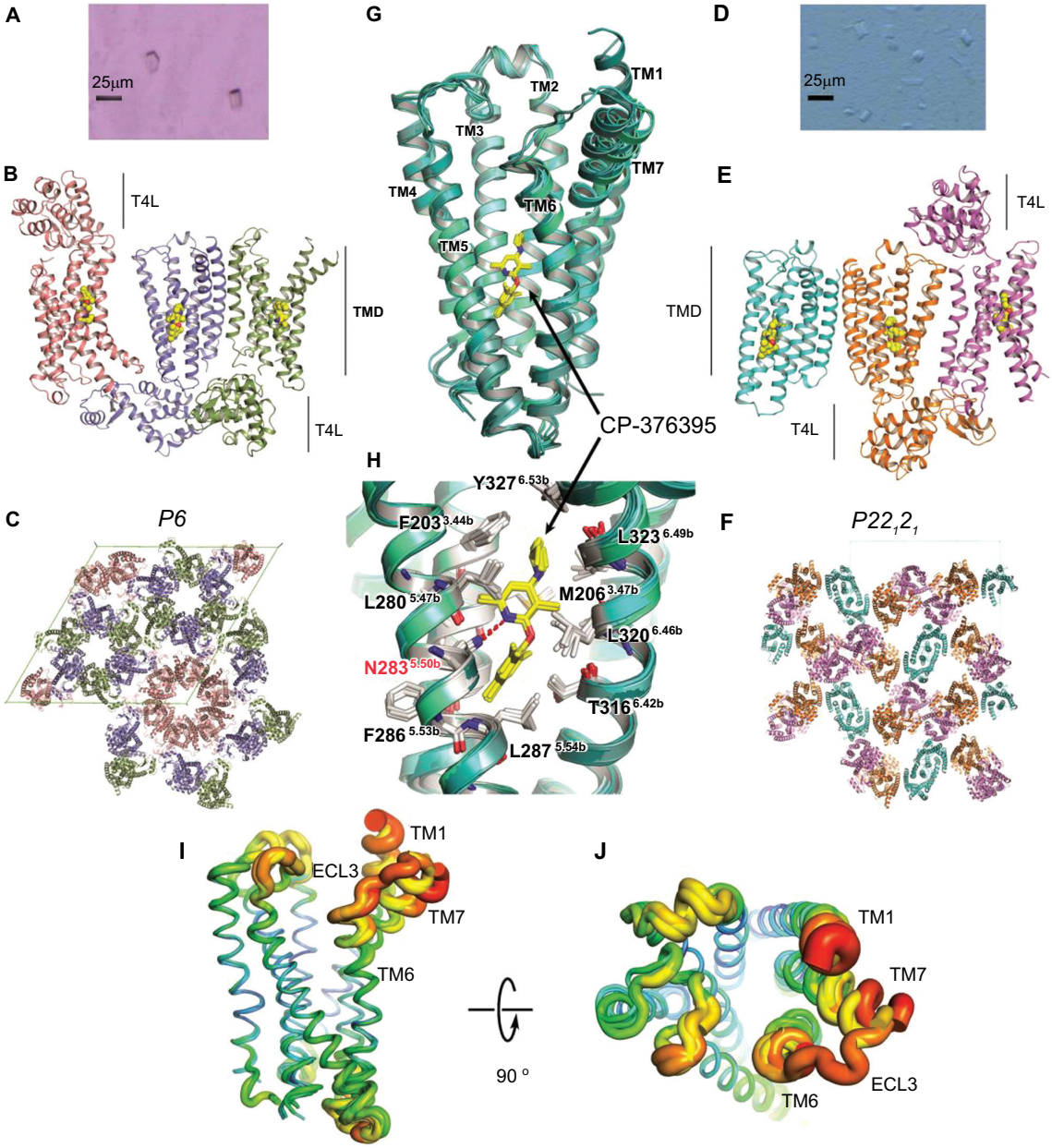

Fig. (1). Overview of the CRF$_1$R crystal structures solved in complex with CP-376395. A - *Left*) Crystals grown in lipidic cubic phase of CRF$_1$R-#76 – hexagonal setting. **B**) The overall structure of CRF$_1$R-#76 solved with three copies in the asymmetric unit. CRF$_1$R-T4L fusion is shown in ribbon representation and coloured by chain, pink, blue and green. The CP-376395 small-molecule is depicted in space fill representation with carbon, nitrogen and oxygen atoms coloured yellow, blue and red respectively. CRF$_1$R-TMD and T4L fusions are denoted. **C**) Crystal packing of CRF$_1$R in the hexagonal setting – view down unique *c* axis. Receptor copies coloured as in (B). **D** - *Right*) Crystals grown in lipidic cubic phase of CRF$_1$R-#105 – orthorhombic setting. **E**) The overall structure of CRF$_1$R-#105 solved with three copies in the asymmetric unit. CRF$_1$R-T4L fusion is shown in ribbon representation and coloured by chain, pink, blue and green. The CP-376395 small-molecule is depicted in space fill representation coloured as in (B), CRF$_1$R-TMD and T4L fusions are denoted. **F**) Crystal packing of CRF$_1$R in the orthorhombic setting – view down *a* axis. Receptor copies coloured as in (B). **G** - *Centre*) Superposition of all 6 CRF$_1$R-TMD copies in ribbon representation coloured in varying shades of cyan as viewed from a plane parallel to the membrane. TM helices are labeled. CP-376395 is labeled and shown in stick representation coloured as in B. **H**) Close-up view of the induced-fit small-molecule allosteric site in CRF$_1$R – receptor copies coloured as in (G). Important receptor residues are labeled and shown in stick representation with carbon, nitrogen and oxygen atoms coloured white, blue and red respectively. CP-376395 is labeled and shown in stick representation coloured as in B. Hydrogen bonds depicted as dashed red lines. **I**) Superposition of all 6 CRF$_1$R-TMD copies as in (G) shown in sausage representation coloured using a relative B-factor spectrum, blue=low; red=high. **J**) Representation as in (I) rotated to view from extracellular space.

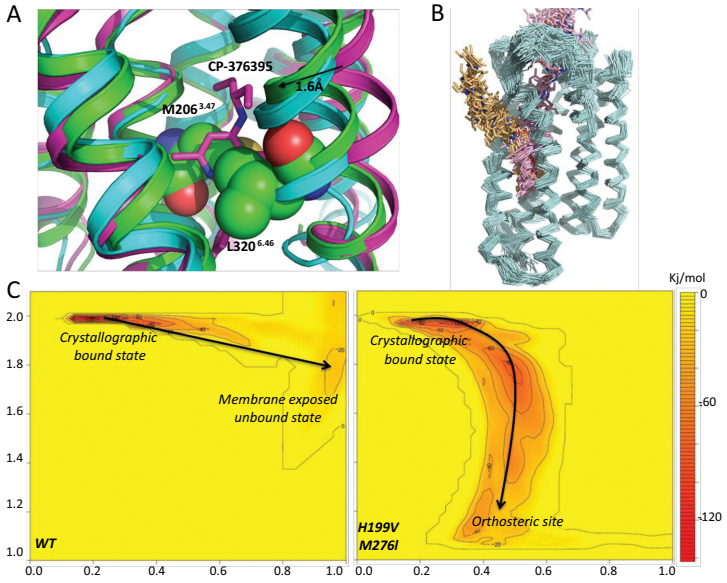

Fig. (2). Analysis of CP-376395 binding to CRF_1R. **A**) Comparison of CP-376395-CRF_1R^{P22121} complex (in magenta), *apo* CRF_1R^{P22121} (in green) and GCGR crystal structure (in cyan). Residues $M206^{3.47}$ and $L320^{6.46}$ are shown in space fill representation with carbon, nitrogen and oxygen atoms coloured green, blue and red respectively. CP-376395 is shown in stick representation with carbon, nitrogen and oxygen atoms coloured magenta, blue and red respectively **B**) The two predicted ligand binding paths are compared, in pink starting from the orthosteric site and in yellow from within the membrane. Binding paths are shown using snapshots of the ligand position during the simulation of binding and dissociation. The protein backbone is shown in cyan as ribbon. **C**) Free energy landscape predicted by the WTMetaD simulation for the dissociation event of CP-376395 in the wild type receptor (left) and in the double mutant H199V, M276I (right). Y axis represents the path CV defining the position on the path, while the X axis the distance from the path CV. The free energy surface is colour-coded from yellow to red (0 to -137 kJ/mol) and the positions of the bound and dissociated states are indicated.

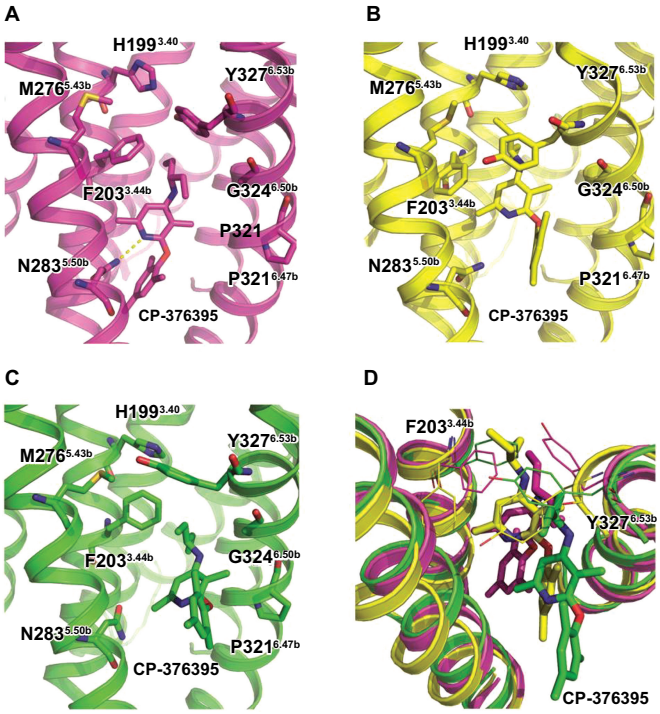

Fig. (3). Key conformations identified during the WTMetaD ligand dissociation path. The ligand and relevant receptor residues are shown in stick representation. $N283^{5.50}$ provides the only H-bond with the CP-376395 ligand while $G324^{6.50}$ and $P321^{6.47}$ modulate the bent trajectory of TM6. $F203^{3.44}$ and $Y327^{6.53}$ change rotameric states during ligand dissociation and are controlled by $M276^{5.44}$ and $H199^{3.40}$. In CRF_2R these two residues are an $I272^{5.44}$ and $V195^{3.40}$ respectively. **A**) CP-376395 in the bound crystallographic conformation. **B**) Predicted first step in CP-376395 dissociation associated with breaking the H-bond with $N283^{5.50}$ and changes in the conformation of $F203^{3.44}$ and $Y327^{6.53}$ to permit initial movement of the ligand toward the extracellular side of the receptor. **C**) The CP-376395 exit route between TM5 and TM6 close to $G324^{6.50}$ and $P321^{6.47}$. **D**) Comparison of the three ligand dissociation states (starting in magenta, first step in yellow and final step in green). The movement of $F203^{3.44}$ and $Y327^{6.53}$ are depicted in line representation.

observed flexibility of ECL3 and any potential structural role in the context of the full-length receptor, a full-length model using the CRF_1R^{P22121} TMD and the crystal structure of the extracellular domain (ECD) (PDB ID: 3EHS) [22] was built. The 6 residues (E109 to V114) connecting the ECD to the TMD of the receptor which are not resolved in any of the available crystal structures have been assumed to be alpha helical and therefore modelled as 1.5 helical turns connecting the C-terminus of the ECD with the N-terminus / top of TM1. The assumption of continuous alpha helix in *ab initio* modelling of these 6 residues, connecting experimentally resolved regions of alpha helix which flank either side, determined the relative orientation of the two protein domains in the final full-length CRF_1R model.

The conformational stability between the CRF_1R –TMD and ECD was initially analyzed using a standard MD simulation within an explicit water-membrane environment. In the starting conformation the main interactions between the two domains are between ECL3 of the receptor TMD and Loop 2 of the ECD. During the 50 ns MD simulation the ECD changed its relative position to adopt a final "closed" conformation on top of the receptor TMD. In the final state model Loop 1, Loop 2 and the C-terminus of the ECD adopt a position closer to ECL1 and ECL2 of the TMD. After structural superimposition of the starting and final state full-length models using the TMD regions only, the Cα RMSD for the ECDs was ~18 Å, with a maximum change for Loop 3 in the ECD greater than 45 Å. In order to identify the most stable "open" and "closed" conformations of the ECD in the full length receptor the system was analyzed using a WTMetaD protocol.

The analysis highlighted the potential integral role of charged residues and electrostatic interactions in mediating interactions in the juxtamembranous (JM) region connecting TM1 to the ECD, and between ECL3 of the TMD to the ECD in controlling the relative position of the two CRF_1R domains. In the "open" conformation D337 and E338 within ECL3 form salt bridges with ECL2 (R263) and the ECD (R76) respectively. In addition $R341^{7.35b}$ interacts with E108 in the JM region (Fig. **4**-**C**) and together with the adjacent E109, K110, K111 and K113 appears to play a key role in stabilizing the full-length receptor "open" state. In the "closed" conformation the JM region partially unwinds allowing D337 in ECL3 to interact with R76 and K113. These interactions result in a stable position of the ECD over the TM helical bundle occluding the entrance to the orthosteric site further locking full-length CRF_1R in the "closed" conformation (Fig. **4**-**D**).

4. DISCUSSION

The crystal structure of the CRF_1R TMD in a hexagonal setting represents a doubling of the structural information that exists for this receptor in the public domain. That the CRF_1R^{P6} and CRF_1R^{P22121} structures are in close agreement in terms of structural superposition of the TMD regions, with molecular features maintained across crystal systems / fundamentally different lattices (and exhibit a comparable and extremely stable dynamics behaviour) further increases confidence that the molecular features of the ground state of the receptor TMD are captured across these structures. Additionally the structure of the human class B glucagon receptor TMD was reported at 3.4 Å resolution in 2013 in complex with the antagonist NNC0640 [40]. Though the position of NNC0640 was not determined in the glucagon crystal structure, superposition of the TMD of CRF_1R and glucagon receptors demonstrates considerable structural conservation of the canonical 7TM helix arrangement (particularly over TMs 1-5) [1]. Taken together this represents a reliable structural framework from which to investigate the complexity of the inactive CRF_1R conformation, and potentially multidomain class B receptors in general. Additionally insight can be gained into the nature of the CRF_1R small-molecule allosteric binding site, the protein conformational changes required for the ligand binding event and potential implications for selectivity. Finally, a molecular model of full-length CRF_1R in the inactive state has been assembled and optimized using unbiased and biased MD.

MD simulation using an *apo* CRF_1R model strongly suggests that the allosteric pocket (found deep towards the intracellular side of the receptor) is induced by ligand binding (Fig. **2**-**A**). Steered MD supports two possible access routes for the ligand to the induced-fit site in CRF_1R: one from the putative orthosteric site in the extracellular side of the receptor and a second from within the membrane, in a location close to TM5 and TM6 (Fig. **2**-**B**). WTMetaD analysis of the free energy surface of the ligand dissociation suggests that the lowest energy escape route for the ligand from the induced-fit pocket is between TM5 and TM6 toward the membrane (Fig. **2**-**C**). During ligand dissociation $F203^{3.44b}$ and $Y327^{6.53b}$ change rotameric states (Fig. **3**-**D**) permitting exit of the small-molecule from the CRF_1R-TMD in a region close to $G324^{6.50b}$ and $P321^{6.47b}$ (Fig. **3**-**C**). These predicted conformational changes required for ligand binding and dissociation also provide a potential rationale for the selectivity of CP-376395 to the human CRF_1R subtype. The functional antagonist activity of CP-376395 for CRF_1R is 12 nM, while >10000 nM for CRF_2R [3]. Sequence identity within the helical bundle between the receptor subtypes is high (78%) and residues participating in direct interactions with CP-376395 in CRF_1R are completely conserved in CRF_2R. Across the second shell of residues in proximity of CP-376395 (less than 5 Å) only two residues differ between CRF_1R and CRF_2R, these being $H199^{3.40b}$ and $M276^{5.43b}$ corresponding to $V195^{3.40b}$ and $I272^{5.43b}$ respectively. Mutation of these residues in CRF_1R to the corresponding amino acids in CRF_2R has been demonstrated to reduce the binding affinity of standard non-peptide antagonists in CRF_1R while concomitantly having little effect on peptide ligand binding [38, 39]. From the WTMetaD simulation $M276^{5.44b}$ and $H199^{3.40b}$ appear to play a crucial role in modulating the conformational changes of $F203^{3.44b}$ and $Y327^{6.53b}$ required for CP-376395 binding / dissociation. In CRF_2R the corresponding $V195^{3.40b}$ and $I272^{5.43b}$ may potentially lock $F^{3.44b}$ and $Y^{6.53b}$ in a conformation incompatible with CP-376395 gaining access to the induced-fit allosteric site.

The ECD of CRF_1R has been shown previously to act as an intrinsic negative regulator of receptor activity, with ECL3 of the TMD playing an important role in mediating crosstalk with the ECD [41, 42]. Using a full-length CRF_1R model and WTMetaD protocol, representative low energy conformations of the ECD in "open" and "closed" states

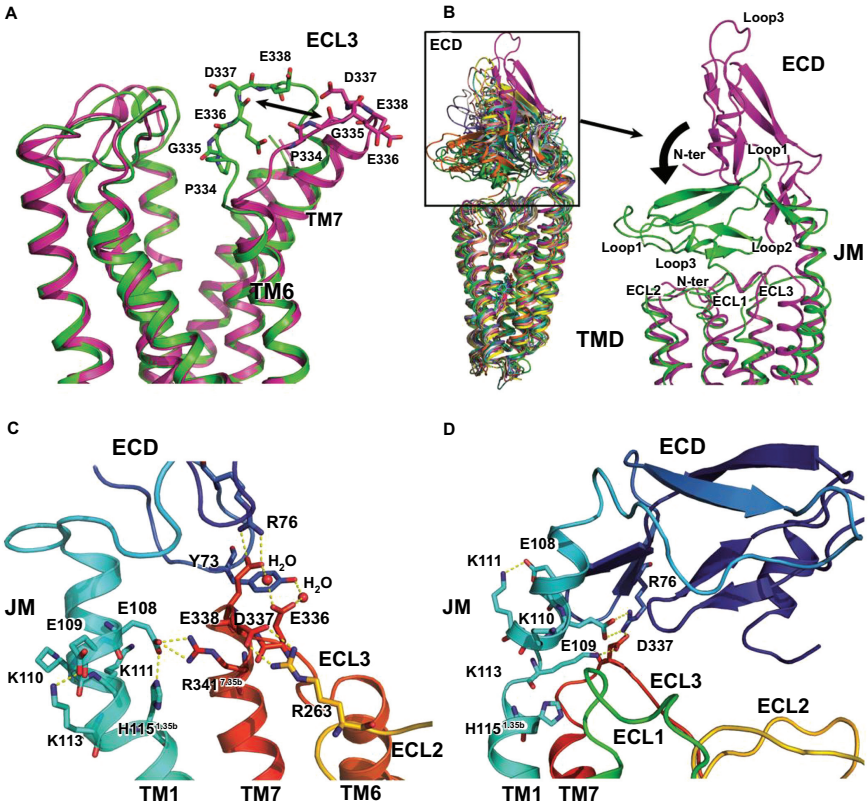

Fig. (4). Analysis of the extracellular surface of CRF_1R. A) Side view of the extracellular region of the CRF_1R receptor TMD highlighting the flexibility of ECL3 during MD simulation. Residues predicted to be crucial in determining the loop flexibility are shown in stick representation. **B**) On the left, superimposition of different snapshots from MD simulation of ECD-CRF_1R^{P22121}. On the right, comparison between the starting (in magenta) and final (in green) conformations of the receptor ECD. Representative lowest energy conformations identified by the WTMetaD protocol for the full length receptor with the ECD in the "open" (**C**) and "closed" (**D**) conformations are shown. Relevant residues are represented as sticks and the backbone as cartoon. The protein is colour coded as rainbow, from blue (N terminus) to red (C terminus). Key interactions are shown as yellow dotted lines.

relative to the TMD have been identified. Mutagenesis, photoaffinity labelling and cysteine trapping studies all provide experimental evidence that in addition to roles played by the extracellular loops, the JM region (connecting TM1 to the ECD) plays an important role in the structure, function and context of full-length multidomain class B receptors [43]. The results presented here implicate electrostatic interactions between ECL3, the ECD, and the JM region as the major determinants in the relative positioning of the two receptor domains. In particular ECL3 appears to play a critical role in mediating interactions between the TMD and the ECD, maintaining the CRF_1R ECD in an inactive "closed" conformation with the receptor TMD, as recently proposed for the glucagon receptor [41]. Studies of the multidomain calcitonin gene related peptide receptor have also previously identified point mutations in ECL3 that result in a significant increase of both basal and ligand-induced activity for this receptor [44]. The result of the WTMetaD highlights the role of E338 from ECL3 in forming a salt bridge with R76 from the ECD, indeed mutagenesis of R76 in CRF_1R to the corresponding residue in either human vasoactive intestinal peptide receptor type 2 (hVIP-R2) or CRF_1R from Xenopus laevis abolishes CRF_1R peptide ligand binding [45]. Finally E336 in ECL3 is predicted to interact with Y73 from loop 2 on the CRF_1R ECD in the "closed" state and mutation of the corresponding residue to alanine in the ECD of the glucagon receptor (Y65A) increases basal activity almost fivefold [41]. Taken together this provides experimental evidence corroborating the modelled interactions in CRF_1R that are important for positioning the ECD relative to the TMD in a functional context. In terms of activation it is possible that following initial binding of the 41 amino acid corticotropin-releasing hormone to the ECD [46, 47], the peptide agonist then relieves receptor inactivation through affecting ECD interactions with ECL3 before subsequently binding to the TMD to induce receptor activation.

CONCLUSION

The structure of CRF_1R in complex with the small molecule CP-376395 at 3.0 Å [9] and in a hexagonal setting at 3.2 Å as presented here have greatly increased our understanding of the architecture of class B receptors including the configuration of the TMD, the open chalice-like nature of the extracellular vestibule and peptidic orthosteric peptide binding pocket and finally the location of a small-molecule induced-fit allosteric pocket deep within the TMD towards the intracellular side of the receptor. The molecular model of full length CRF_1R corroborates the role of the ECD as an intrinsic negative regulator of the receptor activity. To further our

understanding of the mode of action of CRF_1R, and Class B GPCRs in general, structures of the full-length receptor are now required and will represent a significant advance for the field, either in the antagonist close conformation, or in the full agonist state with the corticotropin-releasing hormone (CRH) peptide or a peptide mimetic bound.

Co-ordinates and structure factors have been deposited in the Protein Data Bank under the accession code 4Z9G

AUTHOR CONTRIBUTIONS

A.S.D. designed crystallization constructs, established the platform/protocols for, and carried out LCP crystallization and designed crystal optimization, harvested crystals, collected and processed X-ray diffraction data and refined the structure. R.K.Y.C. performed expression / purification and grew crystals in bicelles, vapour diffusion and collected X-ray diffraction data. K.H. designed and characterized truncation / fusion and crystallisation constructs, established procedures for, and carried out expression and purification, established the platform/protocols for and carried out lipidic cubic phase (LCP) crystallization, collected and processed X-ray diffraction data. R.J.R. solved the novel CRF_1R structure. Computational analysis of the structure and modeling was carried out by A.B. The manuscript was prepared by A.S.D., A.B. and F.H.M.

CONFLICT OF INTEREST

The authors from Heptares Therapeutics declare competing financial interests.

ACKNOWLEDGEMENTS

We thank G. Evans, R. Owen and D. Axford at I24, Diamond Light Source, Oxford, UK for technical support. We thank A. W. Leslie and R. Henderson at the MRC - Laboratory of Molecular Biology, Cambridge, UK. We also thank R. Nonoo and other colleagues at Heptares Therapeutics Ltd. for suggestions and comments. R.J.R is supported by a Principal Research Fellowship from the Wellcome Trust (grant No. 082961/Z/07/Z).

REFERENCES

[1] Bortolato, A.; Doré, A.S.; Hollenstein, K.; Tehan, B.G.; Mason, J. S.; Marshall, F. H. Structure of Class B GPCRs: new horizons for drug discovery. *Br. J. Pharmacol*., **2014**, *171*, 3132-3145.

[2] Bale, T.L.; Vale, W.W. CRF and CRF receptors: role in stress responsivity and other behaviors. *Annu. Rev. Pharmacol. Toxicol*., **2004**, *44*, 525-557.

[3] Chen, Y.L.; Obach, R.S.; Braselton, J.; Corman, M.L.; Forman, J.; Freeman, J.; Gallaschun, R.J.; Mansbach, R.; Schmidt, A.W.; Sprouse, J.S.; Tingley Iii, F.D.; Winston, E.; Schulz, D.W. 2-Aryloxy-4-alkylaminopyridines: discovery of novel corticotropin-releasing factor 1 antagonists. *J. Med. Chem.,* **2008**, *51*, 1385-1392.

[4] Jacobson, K. A.; Costanzi, S. New insights for drug design from the X-ray crystallographic structures of G-protein-coupled receptors. *Mol. Pharmacol*., **2012**, *82*, 361-371.

[5] Tautermann, C.S.; Seeliger, D.; Kriegl, J.M. What can we learn from molecular dynamics simulations for GPCR drug design? *Comput. Struct. Biotechnol*., **2015**, *13*, 111-121.

[6] Caffrey, M.; Cherezov, V. Crystallizing membrane proteins using lipidic mesophases. *Nat. Protoc*., **2009**, *4*, 706-731.

[7] Kabsch, W. Integration, scaling, space-group assignment and post-refinement. *Acta Crystallogr. D. Biol. Crystallogr*., **2010**, *66*, 133-144.

[8] Hanson, M.A.; Roth, C.B.; Jo, E.; Griffith, M.T.; Scott, F.L.; Reinhart, G.; Desale, H.; Clemons, B.; Cahalan, S.M.; Schuerer, S.C.; Sanna, M.G.; Han, G.W.; Kuhn, P.; Rosen, H.; Stevens, R.C. Crystal Structure of a lipid G protein-coupled receptor. *Science*, **2012**, *335*, 851-855.

[9] Hollenstein, K.; Kean, J.; Bortolato, A.; Cheng, R.K.Y.; Doré, A. S.; Jazayeri, A.; Cooke, R.M.; Weir, M.; Marshall, F.H. Structure of class B GPCR corticotropin-releasing factor receptor 1. *Nature*, **2013**, *499*, 438-443.

[10] Evans, P. R.; Murshudov, G. N. How good are my data and what is the resolution? *Acta Crystallogr. D. Biol. Crystallogr*., **2013**, *69*, 1204-1214.

[11] Collaborative Computational Project, Number 4. The CCP4 Suite: Programs for Protein Crystallography. *Acta Crystallogr. D Biol. Crystallogr.,* **1994**, *50*, 760-763.

[12] McCoy, A.J.; Grosse-Kunstleve, R.W.; Adams, P.D.; Winn, M.D.; Storoni, L.C.; Read, R.J. Phaser crystallographic software. *J. Appl. Cryst.,* **2007**, *40*, 658-674.

[13] Read, R.J.; Adams, P.D.; McCoy, A.J. Intensity statistics in the presence of translational non-crystallographic symmetry. *Acta Crystallogr. D. Biol. Crystallogr.,* **2013**, *69*, 176-183.

[14] Emsley, P.; Lohkamp, B.; Scott, W.G.; Cowtan, K. Features and development of Coot. *Acta Cryst*., **2010**, *D66*, 486-501.

[15] Adams, P.D.; Afonine, P.V.; Bunkóczi, G.; Chen, V.B.; Davis, I. W.; Echols, N.; Headd, J.J.; Hung, L.-W.; Kapral, G.J.; Grosse-Kunstleve, R.W.; McCoy, A.J.; Moriarty, N.W.; Oeffner, R.; Read, R. J.; Richardson, D.C.; Richardson, J.S.; Terwilliger, T. C.; Zwart, P.H. PHENIX: a comprehensive Python-based system for macromolecular structure solution. *Acta Cryst.,* **2010**, *D66*, 213-221.

[16] Murshudov, G.N.; Skubák, P.; Lebedev, A.A.; Pannu, N. S.; Steiner, R.A.; Nicholls, R.A.; Winn, M.D.; Long, F.; Vagin, A.A. REFMAC5 for the refinement of macromolecular crystal structures. *Acta Cryst*., **2011**, *D67*, 355-367.

[17] Afonine, P. V.; Grosse-Kunstleve, R. W.; Echols, N.; Moriarty, N. W.; Mustyakimov, M.; Terwilliger, T. C.; Urzhumtsev, A.; Zwart, P. H.; Adams, P. D. Towards automated crystallographic structure refinement with phenix.refine. *Acta Crystallogr. Bio Crystallogr*., **2012**, 68, 352-367.

[18] Chen V.B.; Arendall W.B. 3rd; Headd, J.J.; Keedy, D.A.; Immormino, R.M.; Kapral G. J.; Murray, L.W.; Richardson, J.S.; Richardson, D.C. MolProbity: all-atom structure validation for macromolecular crystallography. *Acta Crystallogr. D. Biol. Crystallogr.,* **2010**, *66*, 12-21.

[19] Badawi, M.M.; Fadl Alla, A.A.; Alam, S.S.; Mohamed, W.A.; Nasr-Eldin Osman, D.A.; Abd Alrazig Ali, S.A.; Ahmed, E.M.E.; Adam, A.A.; Abdullah, R.O.; Salih, M.A. Immunoinformatics Predication and in silico Modeling of Epitope-Based Peptide Vaccine Against virulent Newcastle Disease Viruses. A*m. J. Infectious Dis. Microbiol*., **2016**, *4*(3), 61-71. The PyMOL Molecular Graphics System, Version 1.7.4 Schrödinger, LLC. Available: http://pubs.sciepub.com/ajidm/4/3/3/index.html

[20] Berman, H. M.; Westbrook, J.; Feng, Z.; Gilliland, G.; Bhat, T.N.; Weissig, H.; Shindyalov, I.N.; Bourne, P.E. The Protein Data Bank. *Nucleic Acids Res.*, **2000**, *28*, 235-242.

[21] Maestro, version 9.8, Schrödinger, LLC, New York, NY, 2014.

[22] Pioszak, A. A.; Parker, N.R.; Suino-Powell, K.; Xu, H. E. Molecular recognition of corticotropin-releasing factor by its G-protein-coupled receptor CRFR1. *J. Biol. Chem*., **2008**, *283*, 32900-32912.

[23] Prime, version 3.6, Schrödinger, LLC, New York, NY, 2014.

[24] Lindorff-Larsen, K.; Piana, S.; Palmo, K.; Maragakis. P.; Klepeis, J.L.; Dror, R.O.; Shaw, D. E. Improved side-chain torsion potentials for the Amber ff99SB protein force field. *Proteins*, **2010**, *78*, 1950-1958.

[25] Wang, J.; Wolf, R.M.; Caldwell, J.W.; Kollman, P.A.; Case, D.A. Development and testing of a general amber force field. *J. Comput. Chem.,* **2004**, *25*, 1157-1174.

[26] Jakalian, A.; Jack, D.B.; Bayly, C.I. Fast, efficient generation of high-quality atomic charges. AM1-BCC model: II. Parameterization and validation. *J. Comput. Chem*., **2002**, *23*, 1623-1641.

[27] Jämbeck, J.P.M.; Lyubartsev A.P. Derivation and systematic validation of a refined all-atom force field for phosphatidylcholine lipids. *J. Phys. Chem. B*, **2012**, *116*, 3164-3179.

[28] Wolf, M.G.; Hoefling, M.; Aponte-Santamaría, C.; Grubmüller, H.; Groenhof, G. g_membed: Efficient insertion of a membrane protein into an equilibrated lipid bilayer with minimal perturbation. *J. Comput. Chem.*, **2010**, *31*, 2169-2174.

[29] Darden, T.; York, D.; Pedersen, L. Particle mesh Ewald: An N·log(N) method for Ewald sums in large systems. *J. Chem. Phys.,* **1993**, *98*, 10089-10092.

[30] Bussi, G.; Donadio, D.; Parrinello, M. Canonical sampling through velocity rescaling. *J. Chem. Phys.,* **2007**, *126*, 014101.

[31] Parrinello, M.; Rahman, A. Polymorphic transitions in single crystals: A new molecular dynamics method. *J. Appl. Phys.,* **1981**, *52*, 7182-7190.

[32] Barducci, A.; Bussi, G.; Parrinello, M. Well-tempered metadynamics: a smoothly converging and tunable free-energy method. *Phys. Rev. Lett.*, **2008**, *100*, 020603.

[33] Tribello, G. A.; Bonomi, M.; Branduardi, D.; Camilloni, C.; Bussi, G. PLUMED 2: New feathers for an old bird. *Comput. Phys. Commun.,* **2014**, *185*, 604-613.

[34] Grubmüller, H.; Heymann, B.; Tavan, P. Ligand binding: molecular mechanics calculation of the streptavidin-biotin rupture force. Science, **1996**, *271*, 997-999.

[35] Branduardi, D.; Bussi, G.; Parrinello, M. Metadynamics with adaptive Gaussians. *J. Chem. Theory Comput*., **2012**, *8*, 2247-2254.

[36] Branduardi, D.; Gervasio, F. L.; Parrinello, M. From A to B in free energy space. J. *Chem. Phys.,* **2007**, *126*, 054103.

[37] Tehan, B.G.; Bortolato, A.; Blaney, F.E.; Weir, M.P.; Mason, J.S. Unifying family A GPCR theories of activation. *Pharmacol. Ther*., **2014**, *143*, 51-60.

[38] Liaw, C.W.; Grigoriadis, D.E.; Lorang, M.T.; De Souza, E.B.; Maki, R.A. Localization of agonist- and antagonist-binding domains of human corticotropin-releasing factor receptors. *Mol. Endocrinol.,* **1997**, *11*, 2048-2053.

[39] Hoare, S.R.; Brown, B.T.; Santos, M.A.; Malany, S.; Betz, S.F.; Grigoriadis, D.E. Single amino acid residue determinants of nonpeptide antagonist binding to the corticotropin-releasing factor1 (CRF1) receptor. *Biochem. Pharmacol*., **2006**, *72*, 244-255.

[40] Siu, F.Y.; He, M.; de Graaf, C.; Han, G.W.; Yang, D.; Zhang, Z.; Zhou, C.; Xu, Q.; Wacker, D.; Joseph, J.S.; Liu, W.; Lau, J.; Cherezov, V.; Katritch, V.; Wang, M.; Stevens, R.C. Structure of the human glucagon class B G-protein-coupled receptor. *Nature*, **2013**, *499*, 444-449.

[41] Koth, C.M.; Murray, J.M.; Mukund, S.; Madjidi, A.; Minn, A.; Clarke, H.J.; Wong, T.; Chiang, V.; Luis, E.; Estevez, A.; Rondon, J.; Zhang, Y.; Hötzel, I.; Allan, B. B. Molecular basis for negative regulation of the glucagon receptor. *Proc. Natl. Acad. Sci. U.S.A*., **2012**, *109*, 14393-14398.

[42] Sydow, S.; Flaccus, A.; Fischer, A.; Spiess, J. The role of the fourth extracellular domain of the rat corticotropin-releasing factor receptor type 1 in ligand binding. *Eur. J. Biochem*., **1999**, *259*, 55-62.

[43] Dong, M.; Koole, C.; Wootten, D.; Sexton, P.M.; Miller, L.J. Structural and functional insights into the juxtamembranous aminoterminal tail and extracellular loop regions of class B GPCRs. *Br. J. Pharmacol.*, **2014**, *171*, 1085-1101.

[44] Barwell, J.; Conner, A.; Poyner, D. R. Extracellular loops 1 and 3 and their associated transmembrane regions of the calcitonin receptor-like receptor are needed for CGRP receptor function. *Biochim. Biophys. Acta,* **2011**, *1813*, 1906-1916.

[45] Wille, S.; Sydow, S.; Palchaudhuri, M.R.; Spiess, J.; Dautzenberg, F.M. Identification of amino acids in the N-terminal domain of corticotropin-releasing factor receptor 1 that are important determinants of high-affinity ligand binding. *J. Neurochem.,* **1999**, *72*, 388-395.

[46] Dong, M.; Pinon, D.I.; Cox, R.F.; Miller, L.J. Importance of the amino terminus in secretin family G protein-coupled receptors. Intrinsic photoaffinity labeling establishes initial docking constraints for the calcitonin receptor. *J. Biol. Chem*., **2004**, *279*, 1167-1175.

[47] Parthier, C.; Reedtz-Runge, S.; Rudolph, R.; Stubbs, M.T. Passing the baton in class B GPCRs: peptide hormone activation via helix induction? *Trends Biochem. Sci*., **2009**, *34*, 303-310.